ITER ECRH/ECCD Capabilities for Extended Physics Applications

G. Ramponi[1], D. Farina[1], M. A. Henderson[2], E. Poli[3], G. Saibene[4], H. Zohm[3]

[1]Istituto di Fisica del Plasma, CNR, Ass. EURATOM-ENEA-CNR, Milano,Italy

[2] CRPP, EURATOM –Confédération Suisse, EPFL, CH-1015, Lausanne, Switzerland

[3] IPP-Garching, Max-Planck-Institut für Plasmaphysik, D-85748 Garching, Germany

[4] EFDA Close Support Unit, Boltzmannstrasse 2, D-85748 Garching, Germany

Total number of pages: 32

Total number of Tables: 6

Total number of Figures: 13

ABSTRACT

The ability of the ITER Electron Cyclotron Wave launchers of driving localized current at various plasma locations is analyzed by means of beam tracing codes, looking at extended physics application of ECCD in ITER and at possible synergy between the two launchers. Calculations for an improved design of the Upper launcher, based on four upper ports and front steering mirrors allowing both optimum focusing of the beams and an extended plasma deposition region, show that narrow, high peak current density profiles may be maintained over the radial range $0.4 \leq \rho_p \leq 0.9$. Calculations for the Equatorial launcher, where the control of the deposition location is achieved by varying the toroidal injection angle β, point out that, due to poor localization and incomplete power absorption at large toroidal angles ($\beta > 40^0$), the power deposition and current drive location by this launcher is limited to $\rho \leq 0.55$. Moreover it is shown that performances close to the center can be improved with a poloidal tilt of the low and top front mirrors. The main aim of this study is to provide guidance to the design of both launchers in order to optimize their performances, depending on the physics application.

Email of G. Ramponi: ramponi@ifp.cnr.it

1. Introduction

The envisaged functions of the ITER-ECRH systems are: i) core heating to access H-mode and reach conditions for Q≥10 operation; ii) on and off-axis current drive for current profile control and steady state operation; iii) generation of well localized current drive for control of MHD instabilities as Neoclassical Tearing Modes (NTMs) and sawteeth. The fulfillment of all the above mentioned tasks in a variety of plasmas requires the ability to drive sufficient and well localized current from the core up to close the plasma edge. Depending on the application, the system will utilize either an upper or equatorial launcher to inject EC beams at a fixed frequency f=170 GHz into the plasma. During the last few years, detailed beam tracing calculations in support of the EC upper launcher design have been carried by means of two beam tracing codes, GRAY **[**1**]** and TORBEAM **[**2**]** to evaluate the performance of the upper launcher for its main goal of NTM stabilization, for a number of different mm-wave designs proposed for the Remote Steering (RS) and the Front Steering (FS) launcher options, as part of EFDA technology tasks. [3,4]. The requirement for a large steering of the poloidal injection angle (~21^0) to cope with the expected variation of the radial location of the q=2 and q=3/2 surfaces ($0.65\leq\rho_p\leq0.93$), ρ_p being the square root of the normalized poloidal flux) in a number of ITER scenarios relevant for NTMs, as well as that of injecting well focused beams with a waist close to the plasma, have been shown to be crucial items for the mm-wave optimization. The FS upper launcher fulfils both these requirements providing a performance in excess of the requirements for the NTM stabilization task [5].

The advantage of the FS with respect to the RS design is that the poloidal steering range and the focusing of the beams are decoupled. A 'new design' for the FS upper launcher based on the possibility of using four ITER upper ports has been proposed [6,7], the Extended Physics Launcher (EPL), aiming at covering an increased range of minor radii compared to the NTMs range, while injecting focused beams with their waist well inside the plasma. It consists of four launchers, each housing eight beams, and two steering mechanisms, positioned at different

heights in the port plug. The two steering mirrors are identified as Upper Steering Mirror (USM) and Lower Steering Mirror (LSM). Since each steering mirror carries 4 beams, each set of 4 mirrors controls up to 16 beams, i.e. up to 13.3 MW. The lower set is dedicated to cover the outer region of the plasma ($0.7 \leq \rho_p \leq 0.93$), while the upper set is dedicated to access radial range $0.4 \leq \rho_p \leq 0.9$.

The main function of the upper launcher remains that to provide sufficient and well localized co-CD for the stabilization of (2,1) and (3,2) NTMs. Based on the modified Rutherford equation, the figure of merit for NTM stabilization is defined as $\eta_{NTM}=J_p/J_{bs}$, J_p being the peak ECCD current density and J_{bs} the local unperturbed bootstrap current density. Moreover a quantitative criterion for NTM complete stabilization, based on a multi-machine fit to experimental data [8,9], i.e., $\eta_{NTM} \geq 1.2$, has been taken as the required performance.

Besides its main goal, the EPL is designed for other physics applications, mainly to aid the Equatorial Launcher (EL) for sawtooth destabilization, requiring to extend the radial range where efficient and localized ECCD may be driven to the q=1 region, i.e., down to $\rho_p \sim 0.4$. Actually, sawtooth activity is expected to be of primary importance for ITER, where, due to the stabilizing effect of alpha particles, quite long periods sawtooth terminated by large crashes are expected to occur [10]. The crash events terminating the long sawtooth free periods can provide seed islands for NTMs [11]. To shorten the sawtooth period (destabilization), localized co-CD just inside the q=1 surface is a possibility [12]. The effectiveness in controlling the sawtooth period depends on the capacity of ECCD to modify the evolution of the magnetic shear at the q=1 surface, i.e. on the spatial derivative of the driven current profile [13,14].

The criterion adopted here to evaluate the capacity of the upper and equatorial launchers to control sawtooth period is based on an analytical condition as given in [14] for a local shear variation of a factor two, i.e., $I_{EC}/ d_\rho^2 \geq I_p(\rho_{q=1}) /2(\rho_{q=1})^2$, I_{EC} being the total driven current, d_ρ the (normalized) full width of the driven current density profile at 1/e, and $I_p(\rho_{q=1})$ the plasma current integrated up to the radius corresponding to q=1. Although this criterion does not take into account the effect of the fast α-particles on sawtooth stability, so that the quantitative

estimate is not expected to be accurate, $\eta_S=I_{EC}/d_\rho^2$ can be taken as figure of merit and used for relative comparison of sawtooth destabilization efficiency.

This work reports an optimization study over launch angles and beam characteristics compatible with the EPL design, as well as a study for the Equatorial Launcher, to evaluate the joint capabilities of the entire ITER-ECRH system for extended physics application.

2. EPL optimization study

Aim of the analysis shown in this Section is to find conditions that optimize the figure of merit for NTM stabilization, $\eta_{NTM}=J_p/J_{bs}$, as well as the figure of merit for local magnetic shear variation $\eta_S=I_{EC}/d_\rho^2$. For given plasma parameters and for fixed toroidal angle trajectories, both figures of merit depend on the 'local' value of $n_{//}$, that depends in turn on i) the choice of an 'optimal' toroidal injection angle β (compromise between high I_{EC}/P_{EC} and small d_ρ), ii) on the local beam size and iii) on the spatial derivative of the poloidal flux function $d\psi/ds$ at the absorption region.

Figure 1(a, b) shows the peak current density as a function of the radial location ρ_p, in case of inductive scenario 2, for different values of the 'fixed' toroidal injection angle β. The poloidal injection angle α of a beam injected from USM (R=6.846 m, Z=4.393 m) has been scanned in the range $44^0 \le \alpha \le 68^0$ and that of a beam injected from LSM (R=6.9 m, Z=4.18 m) in the range $34^0 \le \alpha \le 56^0$. Due to the variation of $n_{//}$ along the trajectories and to the dependence of the EC driven current on local plasma parameters, the choice of 'optimal' angles depends on which deposition region is considered as highest priority. In present case, priority is given to the *q=2* region for LSM and to the region from *q=3/2* up to ρ_p = 0.4 for USM, thus 'optimal' toroidal injection angles resulting from the analysis turn out to be $\beta \sim 20^0$ for a beam injected from USM and $\beta \sim 18^0$ for a beam injected from LSM. It is worthwhile noting that, being the upper row dedicated to cover not only the radial range foreseen for NTMs but also to sawtooth control, the choice of $\beta \sim 20^0$ for USM turns out to be a good choice also for η_S in the radial range where q=1 is expected to occur, i.e. $0.4 \le \rho_p \le 0.6$, as shown in Fig.1 c).

Figure 2 shows the results of beam tracing calculations with GRAY code for two wave beams coming from USM at $\beta=20^0$, $\alpha= 44^0$ and 68^0, and two wave beams injected from LSM at $\beta=18^0$, $\alpha= 34^0$ and 56^0.

Optimization over the beam size has been done by taking into account two sets of circular beams with different waists w_0 and different distances Δ of the waist from the respective steering mirror, as indicated in Table 1. Note that positive Δ means that the beam waist is located in the region toward the plasma, i.e. all the considered beams are convergent. The resulting behavior for the peak current density is shown in Fig.3 (a, b). It is worth noting that the waist of the beam C6_U, that provides the highest J_p values for the upper row, is located at a distance of 2.1 m from USM, i.e. close to the absorption region at ρ_p =0.78, while the waist of the 'best' beam (C3_L) for the lower row is located at a distance of 1.6 m from LSM, i.e., close to the absorption region at *q=2* of scenario 2 and scenario 5.

The optimization over the beam size includes also astigmatic beams, foreseen for a design using circular waveguides. In case of simple astigmatism, the astigmatic beams are characterized by four parameters: two beam waists, w_{01} and w_{02}, in two orthogonal directions in a plane perpendicular to the beam-line, and the distances $\Delta_{1,2}$ of each waist from the steering mirror. The four parameters of the astigmatic beams taken into account are listed in Table II and Table III for the upper and lower steering mirror, respectively.

Figure 4(a, b) shows the peak current density values obtained for two astigmatic beams injected from USM and two astigmatic beams injected from LSM, compared with the values obtained by using circular beams with the same waist w_{01}. It may be noted that some reduction of the peak current density (up to ~32% for the A2_U beam at ρ_p =0.39) occurs, depending on the deposition radius. The reduction is related to the broadening of the current profile, due to the larger beam size in the direction parallel to the component of $\nabla\psi$ at the power absorption region, and depends, for a given plasma equilibrium, on the particular trajectory, as shown in Fig. 5(a, b).

The above analysis, done for the inductive scenario 2 by using GRAY code, answered the purpose of optimizing the peak current density driven by a single beam. However it is foreseen that four beams will be launched by each of the two steering mirrors. Since the four beams do not have the same launching points, and as a consequence do not have the same trajectories, a broadening of the absorption and current profile may be expected due to the fact that the maximum absorption does not take place at the same radial location. By imposing a proper convergence/divergence of the four beams, however, it is possible to reduce this effect. The optimization of the beam convergence has been investigated using TORBEAM code and the results obtained for scenario 2 are shown in Fig. 6(a, b). As it can be seen, the deterioration can be kept below 1% for LSM and below 3% for USM. It may be noted from Fig.6b) that the largest deterioration value for USM occurs at ρ_p = 0.78, i.e., at the region where all the four beams have their waists and the beam superposition is not optimal, while the maximum beam convergence is reached at about the center of the steering range, i.e. for ρ_p =0.65.

3. Efficiency of EPL for NTM stabilization and magnetic shear variation

To evaluate the efficiency of the EPL for (2,1) and (3,2) NTMs stabilization, beside the inductive scenario 2, a hybrid scenario 3a and a low q scenario 5 have been considered. The main parameters of the three reference scenarios that are prone to NTMs are listed in Table IV, while in Fig.7 (a, b, c) the electron temperature, density and q profiles are shown, respectively. It is worth noting that the hybrid scenario 3a has the largest values of the ratio T_e/n_e, i.e., the largest ECCD efficiency at (2,1) and (3,2) radial positions, meanwhile it has the innermost location for q=2 and q=3/2 surfaces and the highest values of the bootstrap current density. The opposite holds for the low q scenario 5.

In Fig. 8(a, b) the behavior of the peak current density obtained by GRAY code is shown for the three scenarios, by launching a circular beam from USM and LSM respectively, at respective ‘optimal’ injection angles. Note that the high peak current density values for the

hybrid scenario in the radial range $0.4 \leq \rho_p \leq 0.5$ are due to tangencies of the beam to the flux surfaces at the absorption region.

The values obtained for η_{NTM} by considering the full available power of 13.3 MW injected from LSM are shown in Table V, while those obtained by considering the same power injected from the USM are shown in Table VI. In the last column of the two Tables are also listed the values of the full width 'd' of the driven current profile at 1/e of its maximum. As expected, the 'best' results for η_{NTM} are obtained by injecting from the LSM, being the beams optimized in order to have their minimum size at a distance of 1.6 m from the mirror, i.e., close to the absorption region at *q=2* of scenario 5 and scenario 2. The values obtained for the stabilization efficiency exceed the threshold $\eta_{NTM}=1.2$ at all relevant surfaces of the three reference scenarios. It follows that NTM stabilization can be achieved by injecting a power $P_{EC} \leq 13$ MW from the lower row, with the advantage of limiting the impact on the fusion gain Q [15]. The highest efficiencies are obtained, as expected, for the inductive scenario 2, requiring, to get $\eta_{NTM}=1.2$, a power $P_{EC}=5.9$ MW for the (2,1) mode and $P_{EC}=9$ MW for the (3,2) mode.

The figure of merit for local magnetic shear variation for 13.3 MW injected from USM in the plasma of scenario 2 is shown in Fig.9**,** where it is compared with $I_p(\rho_p) / 2\rho_p^2$, where $I_p(\rho_p)$ is the plasma current inside the ρ_p surface. Note that the analytical condition for local shear variation of a factor two is always well satisfied. For ρ_p values close to q=1 surface, we can expect a good efficiency of the EPL for sawtooth control, although the above criterion does not take into account the effect of the fast α-particles on sawtooth stability, and more accurate evaluations will require the use of a transport code including a more refined model.

4.Integrated analysis of EL and EPL

Physics priorities for the Equatorial Launcher (EL) are i) core heating to access H mode and to reach Q>10, ii) provide steady state current drive for contributing to the plasma current replacement in DT, D, H and He plasmas, iii) sawtooth control, iv) provide on axis and off-axis co- and cnt-current drive for plasma current profile modifications in order to assist a reversed shear formation or to avoid current holes. All these tasks require the possibility to have well

localized current profiles, both co- and counter, depending on the application, from the core up to ρ_p~0.6. An overlap with the upper launcher is desirable, in order that the integrated system will access any radial position from the plasma core to the edge.

The current design of the EL foresees 1 equatorial port, 24 beams injected from 3 steering mirrors (8 beams/mirror) located at R=9.2 m and z=0.03, 1.21 and 0.62 m, that we call low, top and mid mirror, respectively. The launch is horizontal, with toroidal steering capability between 20^0 and 45^0 [16]. Figure 10 shows the results of beam tracing calculations for three wave beams injected from the three steering mirrors at $\beta=20^0$ and $\alpha= 0^0$.

The deposition radius and the driven current as a function of the toroidal launching angle are shown in Fig. 11(a, b) for the three mirrors. As already pointed out by earlier analysis, see for instance [17], only beams injected from the mid mirror may drive current (I_{EC}~25 kA/MW) at $\rho_p<0.2$ (for $\beta=20^0$).

Moreover, the access range is limited up to $\rho_p\leq0.55$ as, for $\beta\geq40^0$, both trajectories and high $n_{//}$ effects lead to incomplete power absorption. In case of scenario 2, for instance, for $\beta=45^0$, only 80% of the power transmitted from the lower mirror is absorbed by the plasma, ~90% for a beam launched from the other two mirrors.

It should be mentioned that present design does not allow counter current drive, so that 'pure' central heating is not possible. In order to avoid undesirable central plasma current profile peaking, the only possibility is to balance co-ECCD and cnt-ECCD at nearly the same radial location. Figure 12(a, b, c) shows the results obtained in the case of beams injected with positive and negative β, in order to provide both co- and cnt-ECCD, and with fixed poloidal tilt angles $\alpha=\pm10^0$ from the top and low mirrors, in order to drive current in the plasma centre. In this case, quite similar absorption radii and currents are obtained from all the three steering mirrors, and core access is possible from each mirror. Note that quite broad profiles, with respect to the EPL profiles, are obtained for $\beta>20^0$, being the profile width determined mainly by Doppler effect.

In Figure 13 the peak current density and the figure of merit for local shear modification of the EL and the EPL are compared. In the range where the deposition locations of EPL and EL overlap, $0.4 \leq \rho_p \leq 0.55$, the EPL appears more effective for the purpose of localized current drive and sawtooth control.

5. Summary and Conclusions

Beam tracing calculations have been carried out to optimize the performances of a 'new' design of the ITER upper launcher aiming at covering an increased range of minor radii with respect to the NTMs range, as well as for the equatorial launcher. Results showed that the upgraded design of the UL launcher provides good performances for NTM stabilization for the three ITER reference scenarios, i.e., $\eta_{NTM}=1.2$ by injecting a power $P_{EC} < 13$ MW from the lower steering mirror. At the same time, it provides the possibility to drive well-localized current densities up to the q=1 location by injecting the power from the upper steering mirror.

Calculations for the Equatorial launcher, where control of the deposition location is achieved by varying the toroidal injection angle β, showed that the power deposition and current drive location is limited to $\rho \leq 0.55$, due to poor localization and incomplete power absorption at large toroidal angles ($\beta > 40^0$). Central current drive and profile control can be improved with a poloidal tilt $\alpha \sim \pm 10^0$ of the low and top front mirrors. Design modifications to the EL would allow this launcher to provide counter current drive to balance co and counter current drive for central heating and for applications as current profile tailoring, control of minimum and central q in reverse shear scenarios.

Concerning the performances of the integrated system, we note that in the range where the deposition locations of EPL and EL overlap, $0.4 \leq \rho_p \leq 0.55$, the EPL appears more effective for the purpose of localized current drive and sawteeth control.

ACKNOWLEDGMENTS

This work, supported by the European Community, was carried out within the framework of the European Fusion Development Agreement. The views and opinions expressed herein do not necessarily reflect those of the European Commission.

REFERENCES

1. D.FARINA, Fusion Science and Technology, this special issue
2. E. POLI, A. G. PEETERS AND G. V. PEREVERZEV, Comp. Phys. Comm. **136**, 90 (2001).
3. H.ZOHM et al., Journal of Physics Conference Series **25**, 234-242 (2005)
4. G.RAMPONI, D.FARINA, S.NOWAK, Journal of Physics Conference Series **25**, 243-251 (2005)
5. G.RAMPONI, D.FARINA, S.NOWAK, 'Physics Analysis of the ITER ECRH & ECCD Upper Launcher Design for NTM Stabilisation' Report FP06-01 on http://www.ifp.cnr.it/publications/2006.html
6. M.HENDERSON et al., Fusion Science and Technology, this special issue
7. G. RAMPONI et al., Proc. of 14th Workshop on ECE and ECRH, Santorini (Greece), May 2006
8. H. ZOHM, Proc. of 14th Workshop on ECE and ECRH, Santorini (Greece), May 2006
9. R.J. LA HAYE et al., Nuclear Fusion **46**, 451-461 (2006**)**
10. F. PORCELLI, D.BOUCHER, M.N.ROSENBLUTH, Plasma Phys. Control. Fusion **38** 2163–2186, (1996)
11. O. SAUTER et al., Phys.Rev.Lett. 88, 105001 (2002)
12. C. ANGIONI et al., Nuclear Fusion 43, 455-468 (2003)
13. J.P. GRAVES et al., Plasma Phys. Control Fusion 47, B121-B123, (2005)
14. A. MERKULOV et al., Proc. of the Joint Varenna-Lausanne Int. Workshop on Theory of Fusion Plasmas, Varenna, p.279, (2004)
15. O. SAUTER and H. ZOHM, Proc. 26th EPS Conf. Plasma Physics,Tarragona, ECA, Vol. **29C** P-2.059 (2005).
16. K. TAKAHASHI et al, Journal of Physics: Conference Series **25** 75-83 (2005)
17. F. VOLPE, Journal of Physics: Conference Series **25** 283-295 (2005)

TABLES

TABLE I. Circular beams parameters

Beam	w_0 (cm)	Δ (cm)	Beam	w_0 (cm)	Δ (cm)
C1_L	1.7	123	C4_U	2.1	152
C2_L	1.9	143	C5_U	2.5	185
C3_L	2.1	162	C6_U	2.9	213

TABLE II. Astigmatic beams from USM

Beam	w_{o1} (cm)	Δ_1 (cm)	w_{o2} (cm)	Δ_2 (cm)
C_U	2.9	212	2.9	212
A1_U	2.9	212	1.7	111
A2_U	2.9	213	1.3	78

TABLE III. Astigmatic beams from LSM

Beam	w_{o1} (cm)	Δ_1 (cm)	w_{o2} (cm)	Δ_2 (cm)
C_L	2.1	153	2.1	153
A1_L	2.1	153	1.8	130
A2_L	2.1	153	1.4	86

TABLE IV. Reference Scenarios parameters

Scenario	I_p (MA)	β_N	n_{e0} (10^{20} m^{-3})	T_{e0} (keV)	$\rho_{2/1}$	J_{boos} ($\rho_{2/1}$) (MA/m^2)	$\rho_{3/2}$	J_{boos} ($\rho_{3/2}$) (MA/m^2)
EOB2	15	1.8	1.02	24.8	0.872	0.073	0.764	0.094
EOB3a	12	2.2	0.86	31.8	0.835	0.120	0.734	0.147
EOB5	17	2.1	1.24	29.5	0.900	0.096	0.810	0.111

TABLE V. NTM stabilization efficiency for 13.3 MW from LSM

Scenario	q	α	J_{peak} MA/m^2	η_{NTM}	d (cm)
EOB2	2	48.2	0.196	2.68	2.9
"	3/2	52.0	0.166	1.77	4.9
EOB3a	2	49.0	0.238	1.98	4.1
"	3/2	56.2	0.191	1.30	6.5
EOB5	2	36.0	0.157	1.63	2.7
"	3/2	47.0	0.150	1.35	3.9

TABLE VI. NTM stabilization efficiency for 13.3 MW from USM

Scenario	q	α	J_{peak} MA/m^2	η_{NTM}	d (cm)
EOB2	2	48.2	0.133	1.82	5.2
“	3/2	57.2	0.157	1.67	6.4
EOB3a	2	54.5	0.183	1.52	6.4
“	3/2	60.2	0.198	1.35	7.8
EOB5	2	43.5	0.095	0.99	5.1
“	3/2	53.0	0.123	1.11	6.0

FIGURES

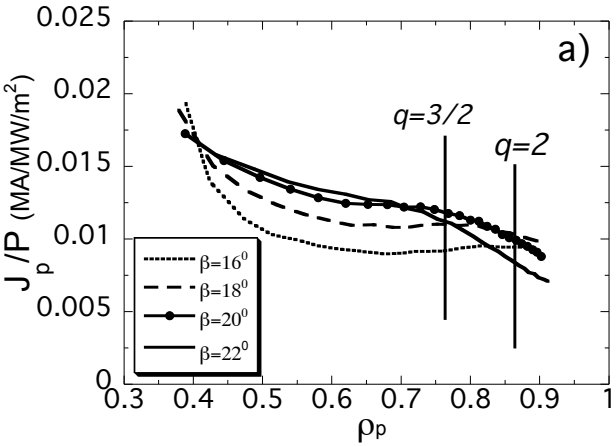

Fig.1a)

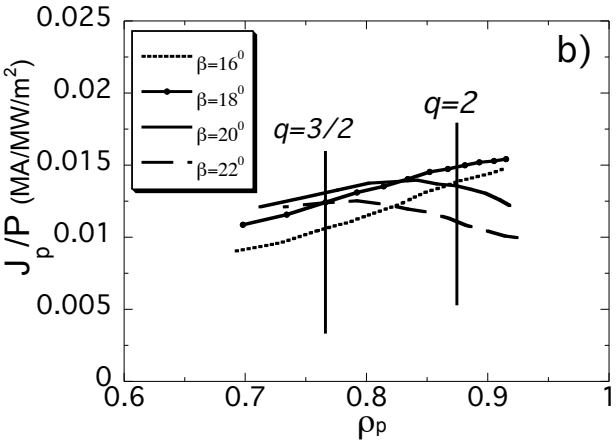

Fig.1b

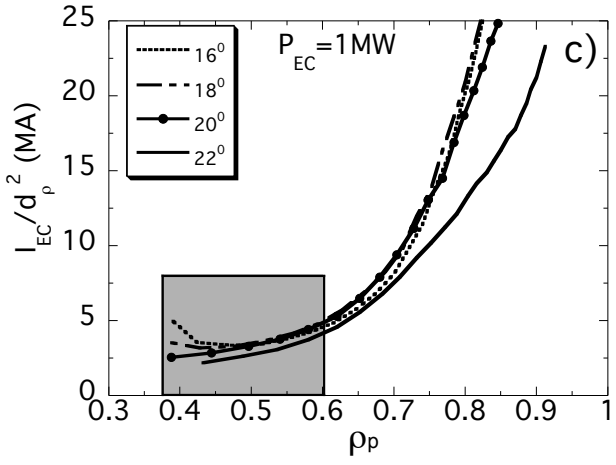

Fig.1c)

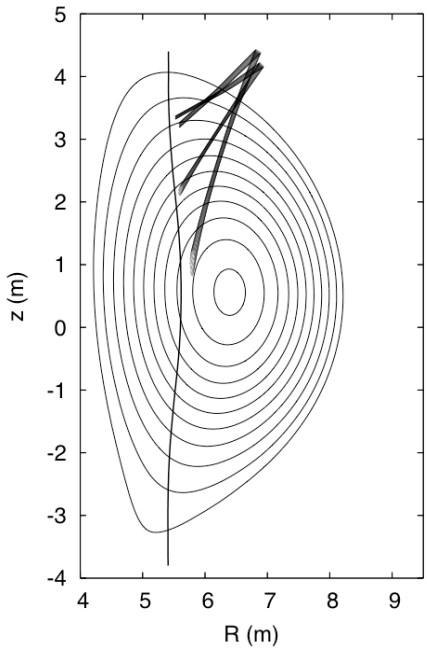

Fig.2

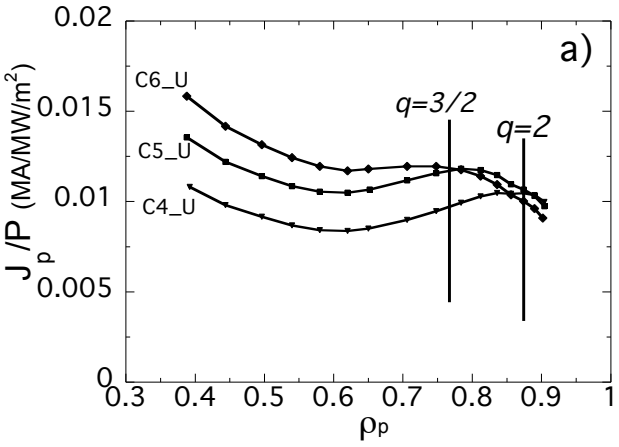
a)
C6_U
C5_U
C4_U
q=3/2
q=2
J /P (MA/MW/m²)
p
ρp
0.02
0.015
0.01
0.005
0
0.3
0.4
0.5
0.6
0.7
0.8
0.9
1

Fig.3a)

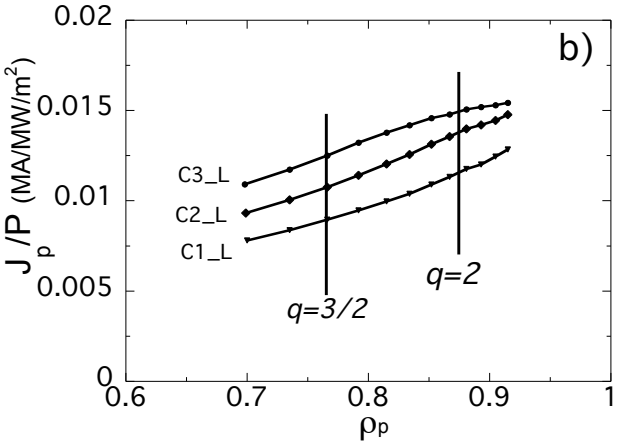
b)
C3_L
C2_L
C1_L
q=3/2
q=2
J /P (MA/MW/m²)
p
ρp
0.02
0.015
0.01
0.005
0
0.6
0.7
0.8
0.9
1

Fig.3b)

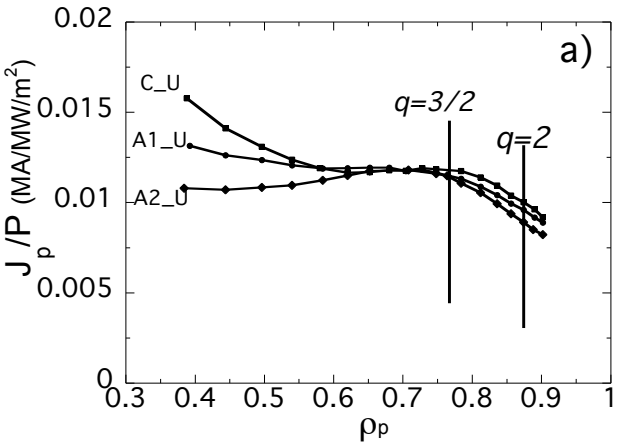
a)
C_U
A1_U
A2_U
q=3/2
q=2
J /P (MA/MW/m²)
p
ρp
0.02
0.015
0.01
0.005
0
0.3
0.4
0.5
0.6
0.7
0.8
0.9
1

Fig.4a)

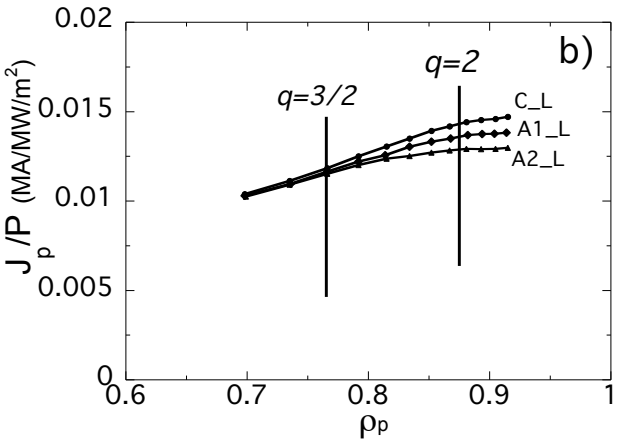
b)
q=2
q=3/2
C_L
A1_L
A2_L
J /P (MA/MW/m²)
p
ρp
0.02
0.015
0.01
0.005
0
0.6
0.7
0.8
0.9
1

Fig.4b)

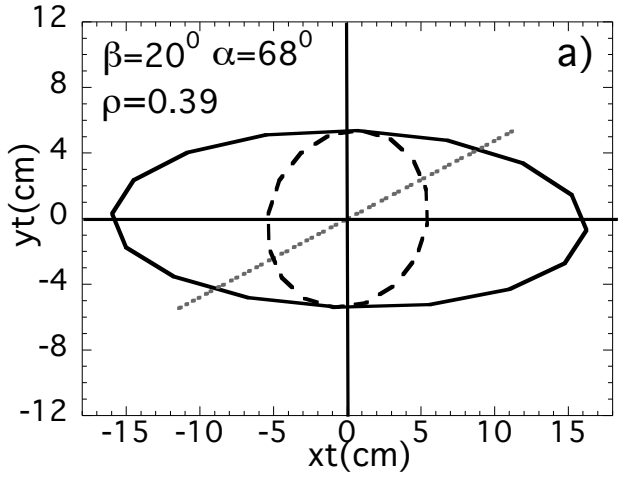
β=20⁰ α=68⁰
ρ=0.39
a)
yt(cm)
xt(cm)
12
8
4
0
-4
-8
-12
-15
-10
-5
0
5
10
15

Fig.5a)

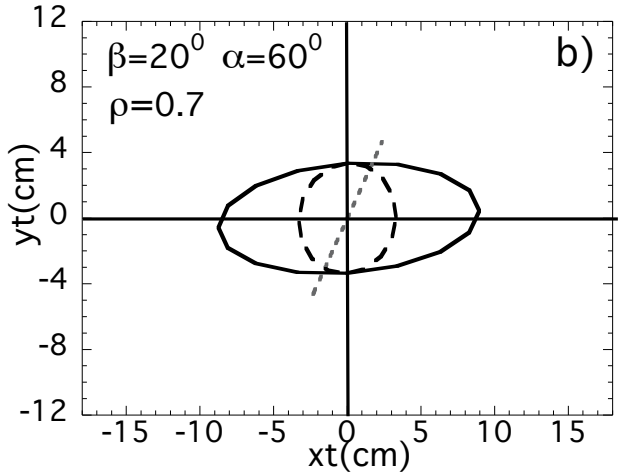
β=20⁰ α=60⁰
ρ=0.7
b)
yt(cm)
xt(cm)
12
8
4
0
-4
-8
-12
-15
-10
-5
0
5
10
15

Fig.5b)

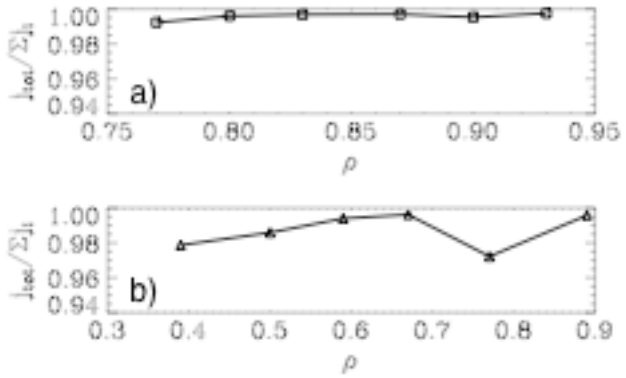
1.00
0.98
0.96
0.94
a)
0.75
0.80
0.85
0.90
0.95
ρ
1.00
0.98
0.96
0.94
b)
0.3
0.4
0.5
0.6
0.7
0.8
0.9
ρ

Fig. 6(a, b)

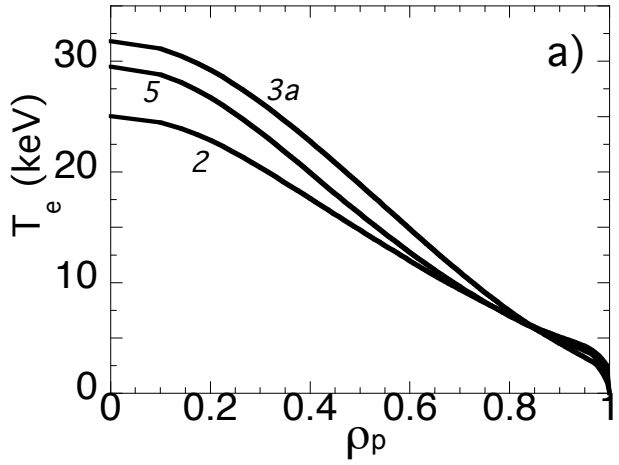

Fig.7a)

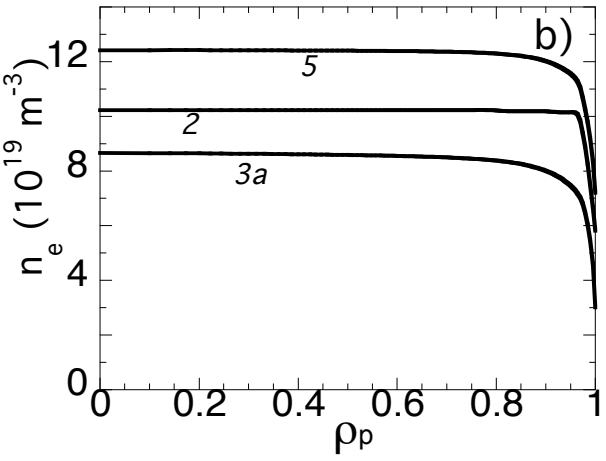

Fig.7b)

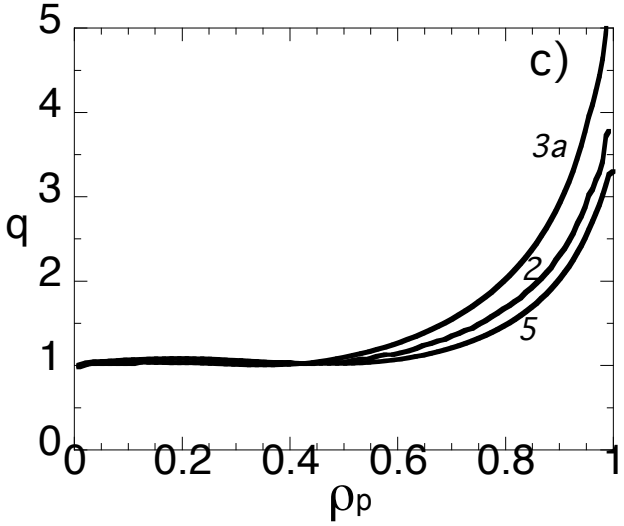

Fig.7c)

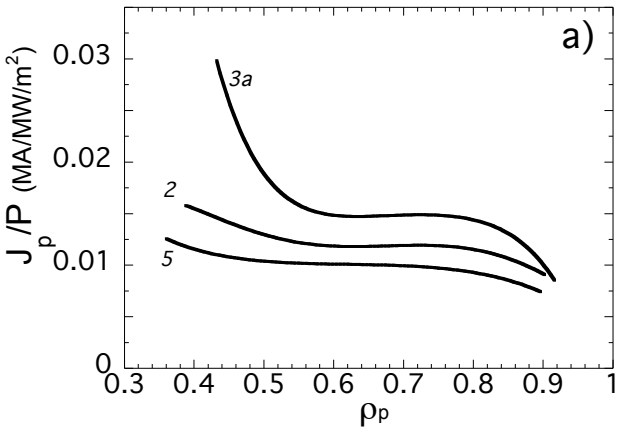
a)
3a
2
5
0.03
0.02
0.01
0
0.3
0.4
0.5
0.6
0.7
0.8
0.9
1
J /P (MA/MW/m2)
p
ρp

Fig.8a)

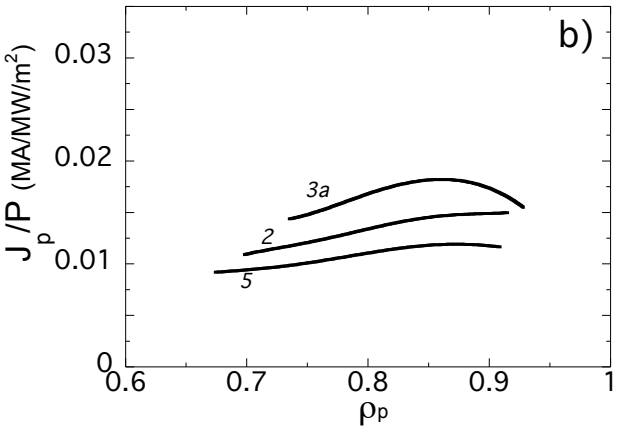
b)
3a
2
5
0.03
0.02
0.01
0
0.6
0.7
0.8
0.9
1
J /P (MA/MW/m2)
p
ρp

Fig.8b)

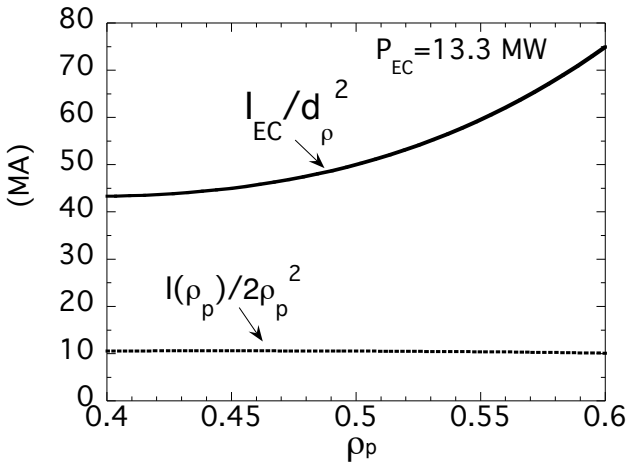
80
70
60
50
40
30
20
10
0
(MA)
0.4
0.45
0.5
0.55
0.6
ρp
P_EC=13.3 MW
I_EC/d_ρ^2
I(ρ_p)/2ρ_p^2

Fig.9

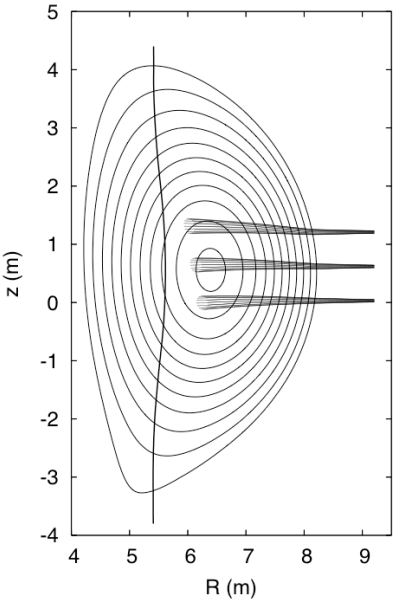

Fig.10

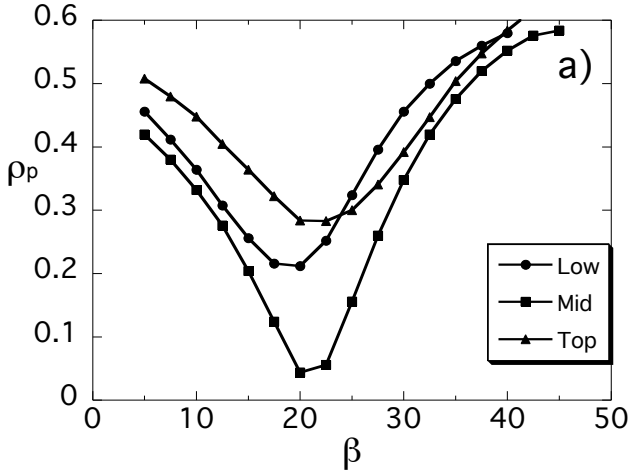

Fig.11a)

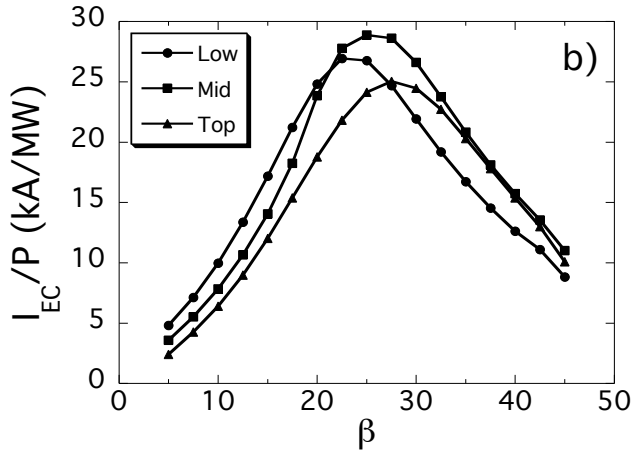

Fig.11b)

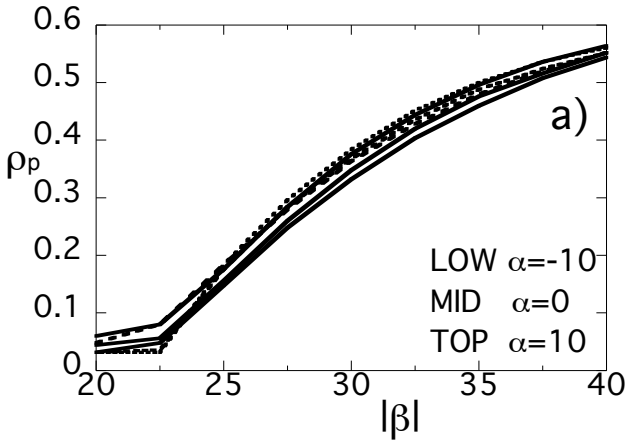

Fig.12a)

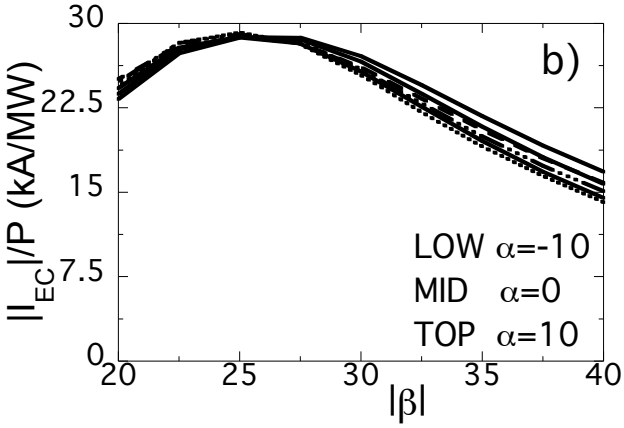

Fig.12b)

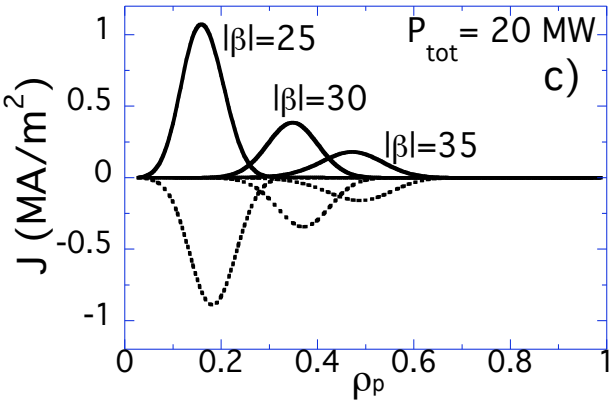

Fig.12c)

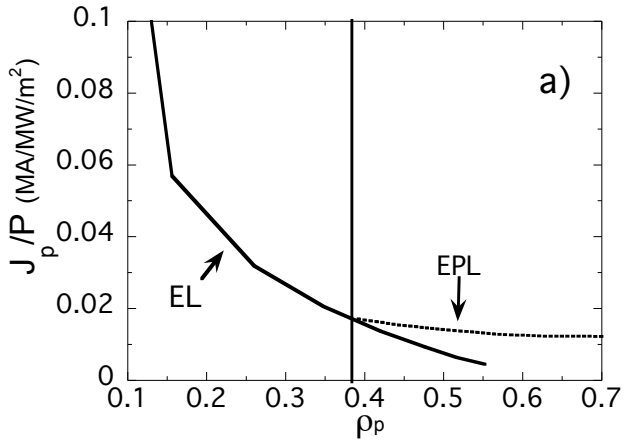

Fig.13a)

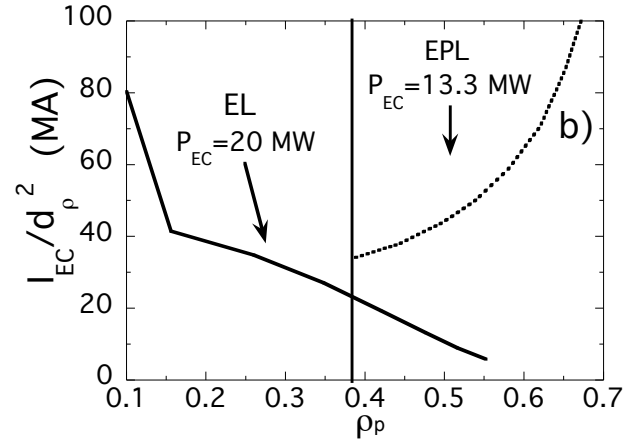

Fig.13b)

FIGURE CAPTIONS

FIGURE 1(a, b, c). Peak current density for toroidal angle β values in the range 16^0–22^0 as a function of its location a) for injection from the USM, scanning the poloidal steering angle α in the range 44^0-68^0, b) for injection from the LSM, scanning α in the range 34^0-56^0 c) figure of merit for sawtooth control for 1 MW of power injected from USM, scanning the launching angles in the same ranges as in case a). The shaded region indicates where the q=1 surface is likely to occur.

FIGURE 2. Results from beam tracing calculation with GRAY code for two wave beams coming from USM at $\beta=20^0$, $\alpha= 44^0$ and 68^0, and two wave beams injected from LSM at $\beta=18^0$, $\alpha= 34^0$ and 56^0. Closed curves are normalized poloidal flux surfaces of ITER scenario 2 at the end of burning, while the quasi-vertical line indicates the cold resonance for EC waves at a frequency f=170 GHz.

FIGURE 3. Peak current density values obtained by scanning the waist of circular beams as given in Table I injected a); from the USM at $\beta=20^0$; b) from the LSM at $\beta=18^0$.

FIGURE 4 (a, b). Comparison of the peak current density values for the astigmatic beams A1_U, A2_U and the circular beam C_U injected from USM at $\beta=20^0$ a); for the astigmatic beams A1_L , A2_L and the circular beam C_L injected from LSM at $\beta=18^0$ b).

FIGURE 5 (a, b). Beam cross sections, at $1/e^2$ of the power, of the C_U beam (dashed circles) and A2_U beam (continuous lines) at the absorption region, for two values of the steering angle α corresponding to power deposition at ρ_p =0.39 a) and at ρ_p =0.7 b). Dotted lines indicate the local direction of $\nabla\psi$.

FIGURE 6(a, b). The ratio between the maximum ECCD current density and the "optimum" current density that would result from a perfect superposition of the four beams, for the lower (a) and the upper (b) steering mirror. ITER Scenario 2 is considered.

FIGURE 7(a, b, c). Electron temperature a), density b), and q c) profiles of the three reference scenarios.

FIGURE 8(a, b). Peak current density for the three reference scenarios as a function of its location, a) for injection from the USM at $\beta = 20^0$ scanning the steering angle α in the range 44^0-68^0, b) for injection from the LSM at $\beta = 18^0$ scanning the steering angle α in the range 34^0-56^0.

FIGURE 9. Figure of merit $\eta_S = I_{EC}/ d_\rho^2$ for magnetic shear variation compared with $I_p(\rho_p) /2\rho_p^2$ for 13.3 MW injected from USM in the plasma of scenario 2.

FIGURE 10. Results from beam tracing calculation with GRAY code for three wave beams coming from the 3 steering mirrors of the EL at $\beta=20^0$, $\alpha= 0^0$, for the same scenario of Fig.2.

FIGURE 11(a, b). Power deposition location a) and total driven current per unit power b) for horizontal launch by the 3 rows of the equatorial launcher as a function of the toroidal injection angle.

FIGURE 12(a,b,c). Power deposition location a) and total driven current per unit power b) for tilted top and low mirrors injection, $\alpha=\pm10^0$, as a function of the absolute value of β (continuous lines indicate co-current driven for positive values of β, dotted lines indicate cnt-current driven for negative values of β); co- and cnt-current profiles obtained at $\beta= \pm 25^0, \pm 30^0, \pm 35^0$, for a power of 20 MW c).

FIGURE 13(a, b). Peak current density values per unit power as a function of the normalized poloidal radius for the EPL (taking into account a beam launched from USM) and for the EL (taking into account poloidally tilted top and low beams) a); figure of merit for local shear variation of the EL (for 20 MW), and EPL (for 13.3 MW) b).